In Vivo Assessment of Aqueous Humor Dynamics Upon Chronic Ocular Hypertension and Hypotensive Drug Treatment Using Gadolinium-Enhanced MRI

Leon C. Ho,[1–3] Ian P. Conner,[2,4,8] Chi-Wai Do,[5] Seong-Gi Kim,[1,2,4,6,7,10] Ed X. Wu,[3] Gadi Wollstein,[2,8] Joel S. Schuman,[2,4,6,8–10] and Kevin C. Chan[1,2,4,6,8,10]

[1]NeuroImaging Laboratory, University of Pittsburgh, Pittsburgh, Pennsylvania, United States
[2]UPMC Eye Center, Eye and Ear Institute, Ophthalmology and Visual Science Research Center, Department of Ophthalmology, University of Pittsburgh School of Medicine, Pittsburgh, Pennsylvania, United States
[3]Department of Electrical and Electronic Engineering, The University of Hong Kong, Pokfulam, Hong Kong, China
[4]Department of Bioengineering, Swanson School of Engineering, University of Pittsburgh, Pittsburgh, Pennsylvania, United States
[5]School of Optometry, The Hong Kong Polytechnic University, Hung Hom, Hong Kong, China
[6]McGowan Institute for Regenerative Medicine, University of Pittsburgh, Pittsburgh, Pennsylvania, United States
[7]Center for Neuroscience Imaging Research, Institute for Basic Science, Department of Biological Science, Sungkyunkwan University, Suwon, Korea
[8]Louis J. Fox Center for Vision Restoration, University of Pittsburgh, Pittsburgh, Pennsylvania, United States
[9]Clinical and Translational Science Institute, University of Pittsburgh, Pittsburgh, Pennsylvania, United States
[10]Center for the Neural Basis of Cognition, University of Pittsburgh and Carnegie Mellon University, Pittsburgh, Pennsylvania, United States

Correspondence: Kevin C. Chan, 3025 East Carson Street, Room 159, Departments of Ophthalmology and Bioengineering, University of Pittsburgh, Pittsburgh, PA, USA; chuenwing.chan@fulbrightmail.org.

Submitted: February 28, 2014
Accepted: April 16, 2014

Citation: Ho LC, Conner IP, Do C-W, et al. In vivo assessment of aqueous humor dynamics upon chronic ocular hypertension and hypotensive drug treatment using gadolinium-enhanced MRI. *Invest Ophthalmol Vis Sci*. 2014;55:3747–3757. DOI:10.1167/iovs.14-14263

Purpose. Although glaucoma treatments alter aqueous humor (AH) dynamics to lower intraocular pressure, the regulatory mechanisms of AH circulation and their contributions to the pathogenesis of ocular hypertension and glaucoma remain unclear. We hypothesized that gadolinium-enhanced magnetic resonance imaging (Gd-MRI) can visualize and assess AH dynamics upon sustained intraocular pressure elevation and pharmacologic interventions.

Methods. Gadolinium contrast agent was systemically administered to adult rats to mimic soluble AH components entering the anterior chamber (AC) via blood–aqueous barrier. Dynamic Gd-MRI was applied to examine the signal enhancement in AC and vitreous body upon microbead-induced ocular hypertension and unilateral topical applications of latanoprost, timolol maleate, and brimonidine tartrate to healthy eyes.

Results. Gadolinium signal time courses in microbead-induced hypertensive eyes possessed faster initial gadolinium uptake and higher peak signals in AC than control eyes, reflective of reduced gadolinium clearance upon microbead occlusion. Opposite trends were observed in latanoprost- and timolol-treated eyes, indicative of their respective drug actions on increased uveoscleral outflow and reduced AH production. The slowest initial gadolinium uptake but strongest peak signals were found in AC of both brimonidine-treated and untreated fellow eyes. These findings drew attention to the systemic effects of topical hypotensive drug treatment. Gadolinium leaked into the vitreous of microbead-induced hypertensive eyes and brimonidine-treated and untreated fellow eyes, suggestive of a compromise of aqueous–vitreous or blood–ocular barrier integrity.

Conclusions. Gadolinium-enhanced MRI allows spatiotemporal and quantitative evaluation of altered AH dynamics and ocular tissue permeability for better understanding the physiological mechanisms of ocular hypertension and the efficacy of antiglaucoma drug treatments.

Keywords: gadolinium, magnetic resonance imaging, aqueous humor dynamics, ocular tissue permeability, intraocular pressure

Glaucoma is an irreversible neurodegenerative disease of the visual system[1–5] and is the second leading cause of blindness in the world.[6] As elevation of intraocular pressure (IOP) is the major risk factor for glaucoma, all approved clinical strategies to manage glaucoma target lowering IOP by altering aqueous humor dynamics.[7] Antiglaucoma agents may lower IOP through different mechanisms that include suppressing aqueous humor formation or inflow, facilitating aqueous humor drainage or outflow, or the combination of both. However, the exact regulatory mechanisms of aqueous humor circulation and the contributions of imbalanced aqueous humor dynamics to the pathogenesis of ocular hypertension and glaucoma are not fully elucidated.

Several techniques have been able to trace aqueous humor dynamics, such as anterior chamber infusion and the use of radioactive and fluorescent tracers.[8–12] However, most of these

techniques involve invasive procedures that preclude longitudinal monitoring of aqueous humor dynamics due to alterations of normal physiological conditions. Gadolinium (Gd) diethylenetriamine-pentaacetic acid (DTPA) is a passive T1 magnetic resonance (MR) contrast agent clinically approved for assessing blood flow and vascular leakage in the eye,[13–16] the brain,[17–19] and the body.[20,21] Because of its small molecular weight, it can also mimic aqueous humor components and readily pass through the leaky blood–aqueous barrier but not the aqueous–vitreous or blood–retinal barrier in normal adult eyes upon systemic administration.[20,22–28] Gadolinium-enhanced magnetic resonance imaging (Gd-MRI) has been used to demonstrate the entrance of Gd into ciliary body stroma and its passage into the anterior chamber.[20,22,23] Gadolinium does not actively transport to the ocular components and is known to be a passive permeability tracer reflecting the functions of tight junctions between cells.[26] Gadolinium MRI also allows in-depth localization favoring in vivo and longitudinal monitoring of ocular fluid biotransport in different eye components simultaneously.[23–27] In this study, dynamic Gd-MRI was exploited to visualize and quantitatively assess aqueous humor dynamics and ocular tissue permeability in a rat model of microbead-induced chronic ocular hypertension and in healthy, normotensive rats after unilateral topical applications of three ophthalmic hypotensive eye drops known to affect IOP through different processes. The aim was to better understand in vivo and noninvasively the mechanisms of ocular physiology and biotransport as well as their relationships to altered IOP and glaucoma.

Materials and Methods

Animal Preparation

All animal experiments were performed in accordance with the ARVO Statement for the Use of Animals in Ophthalmic and Vision Research and protocols reviewed and approved by the University of Pittsburgh's Institutional Animal Care and Use Committee. Twenty-six adult Sprague-Dawley rats at 8 to 10 weeks old were divided into four groups. For group 1 (microbead [MB]; $n = 8$), the rats received unilateral microbead-induced chronic ocular hypertension to the right eyes. They were first anesthetized by inhalation of a mixture of air and isoflurane (3% for induction and 1.25% for maintenance). Tropicamide (Akorn, Inc., Lake Forest, IL, USA) and proparacaine (Bausch & Lomb, Inc., Rochester, NY, USA) were topically administered to dilate the pupil and anesthetize the surface of the eye. Polystyrene microbeads (Flurospheres; Invitrogen, Carlsbad, CA, USA) were reformulated at a concentration of 2.0×10^7 beads/mL. Five microliters of 15-μm polystyrene microbeads followed by 5 μL of 10-μm microbeads was injected into the anterior chamber by a microinjection system at 12 pounds per square inch (psi) through a sharp glass micropipette (World Precision Instruments, Sarasota, FL, USA) under a surgical microscope so as to occlude the larger pores and then the remaining smaller pores in the trabecular meshwork. An air bubble was injected at the end of the microbead injection in order to push the microbeads into the peripheral anterior chamber and the trabecular meshwork area, and to prevent egress of microbeads after withdrawal of the micropipette. Gentamicin sulfate (Falcon Pharmaceuticals, Ltd., Fort Worth, TX, USA) was topically administered at the end of injection. For groups 2 to 4, the right eyes of 18 healthy, normotensive rats received topical administration of 0.005% latanoprost (Bausch & Lomb, Inc.; group 2; Lat; $n = 6$), 0.5% timolol maleate (Sandoz Canada, Inc., Boucherville, QC; group 3; Tim; $n = 6$), and 0.2% brimonidine tartrate (Bausch & Lomb, Inc.; group 4; BT; $n = 6$) ophthalmic hypotensive solutions at 1 hour prior to MRI experiments. Three weeks after MRI experiments on groups 2 to 4, saline was topically applied to the right eyes of two rats randomly selected from each group (Sal; $n = 6$) as sham control, and the same Gd-MRI procedures were repeated.

Intraocular Pressure Measurement

The IOPs of both eyes were measured using the TonoLab rebound tonometer (Colonial Medical Supply, Franconia, NH, USA) under isoflurane gas anesthesia. At least 18 valid IOP values from each eye were obtained and averaged. For rats undergoing microbead-induced chronic ocular hypertension, IOP measurements were performed every 3 days after microbead injection, and MRI experiments were performed 3 weeks after microbead injection. Intraocular pressures were also measured immediately before MRI experiments for all rats under identical procedures.

MRI Protocol

All MRI measurements were performed utilizing a 9.4-Tesla/31-cm Varian/Aglient (Santa Clara, CA, USA) horizontal bore scanner with a transmit–receive volume coil. Rats were anesthetized with isoflurane (3% for induction and 1.5% for maintenance) and kept warm under circulating water during the MRI experiment. Respiration rate was monitored using a small pneumatic pillow (SA Instruments, Inc., Stony Brook, NY, USA). Gadolinium-DTPA (Magnevist, Schering, Germany) was intraperitoneally (i.p.) injected at a dose of 0.3 mmol/kg after one T1-weighted MR image using a fast spin echo sequence was acquired at baseline. T1-weighted MR imaging at 30 seconds temporal resolution was continuously acquired for 2 hours. The imaging parameters were repetition time/echo time = 600/8 ms, echo train length = 8, field of view = 26×26 mm^2, and in-plane resolution = 102×102 μm^2. Seven 1-mm-thick slices were positioned across the globes in a coronal orientation using scout T2-weighted MR images in all coronal, transverse, and sagittal planes as references for reproducible localization.

Data Analysis

In the T1-weighted imaging slice bisecting the center of the globes, regions of interest were manually drawn on the anterior chamber and vitreous body of each eye using ImageJ v1.47 (Wayne Rasband, National Institutes of Health, Bethesda, MD, USA). The averaged time course from each region of interest measurement before and after Gd injection was fitted into a sixth-degree polynomial using MatLab (The MathWorks, Inc., Natick, MA, USA). The peak percentage (%) Gd signal enhancement, time to peak, initial rate of Gd signal increase within the first 10 minutes after Gd injection, and the area under the curve were extracted from the time courses and compared between both eyes of the same groups using two-tailed paired *t*-tests, and across groups using one-way ANOVA and post hoc Tukey's tests. Data are presented as mean ± standard deviation unless otherwise specified. Results were considered significant when $P < 0.05$.

Results

Figure 1 shows the IOP time profiles of the microbead-induced ocular hypertension model, as well as the IOP measurements in both eyes of all groups immediately before MRI experiments. For the microbead group, the IOP of the left control eye

Investigative Ophthalmology & Visual Science

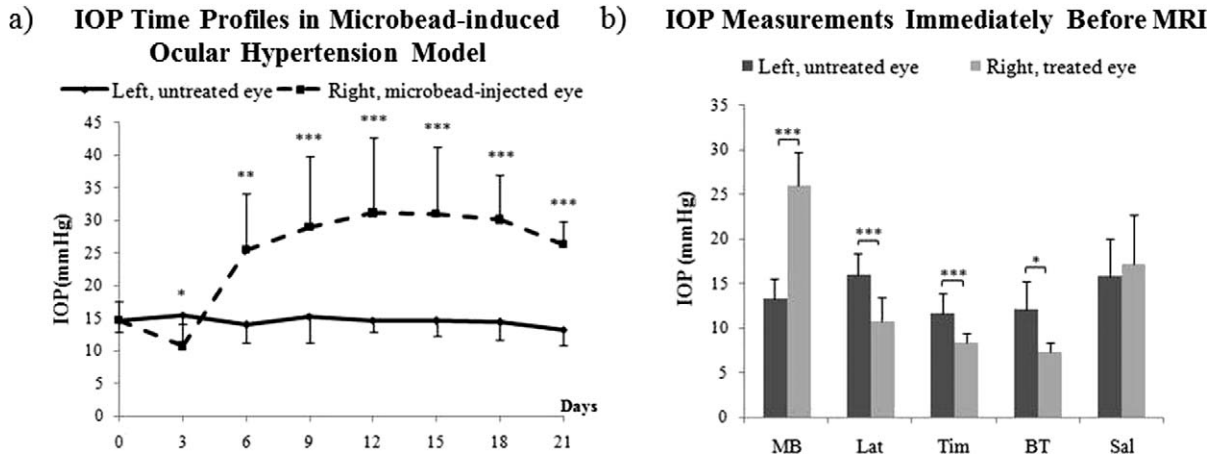

Figure 1. (**a**) Time profiles of IOP in the microbead-induced ocular hypertension rat model from the day of microbead injection (day 0) to 3 weeks after microbead injection (day 21) to the anterior chamber of the right eye. (**b**) Measurements of IOP immediately before MRI experiments on adult rats receiving microbead-induced chronic ocular hypertension (MB, $n = 8$) or topical administrations of latanoprost (Lat, $n = 6$), timolol maleate (Tim, $n = 6$), brimonidine tartrate (BT, $n = 6$), and saline sham control (Sal, $n = 6$) to the right eyes. Microbead occlusion to the right eye significantly elevated IOP by approximately 2-fold compared to the untreated left eye starting at approximately 1 week after microbead injection up to the end of the experimental period at 3 weeks postinjection. Topical administration of latanoprost, timolol, and brimonidine to the right eyes for approximately 1 hour significantly lowered IOP, whereas no apparent effect on IOP was observed upon topical administration of saline (paired *t*-tests between contralateral eyes, $^{*}P < 0.05$, $^{**}P < 0.01$, $^{***}P < 0.001$).

remained stable at approximately 14 mm Hg throughout the experimental period, whereas the right eye receiving microbead occlusion demonstrated a sustained IOP elevation by approximately 2-fold compared to the left control eye starting at 1 week after microbead injection. After ocular hypotensive drug treatment to healthy, normotensive rats, the IOPs of the right eyes treated by latanoprost, timolol, and brimonidine were 11 ± 3, 8 ± 1, and 7 ± 1 mm Hg, respectively, and were significantly lower than in their fellow left control eyes (paired *t*-tests, $P < 0.05$). There was no significant IOP difference in the left eyes among microbead, latanoprost, timolol, brimonidine, and saline sham control groups (ANOVA, $P > 0.05$), or between contralateral eyes in the saline group (paired *t*-test, $P > 0.05$). Figure 2 shows the basic rat eye anatomy and definitions of regions of interest in the anterior chamber and vitreous body in a representative T1-weighted MR image from the saline group temporally averaged at approximately 1 hour after Gd i.p. injection. Figure 3 shows temporally averaged T1-weighted MR images serially at nine different time intervals from the saline group, showing increasing Gd signal enhancement in the anterior chamber of both eyes within the first hour after Gd injection.

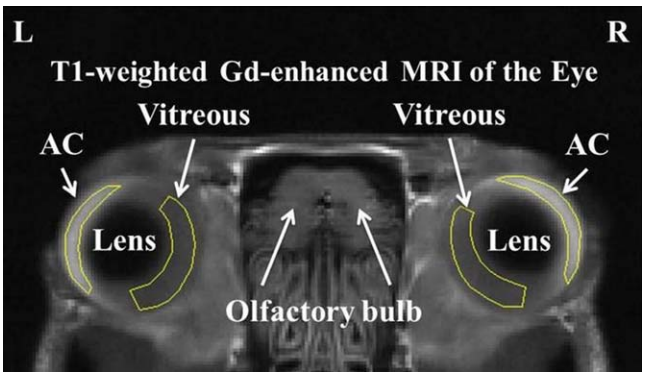

Figure 2. Representative T1-weighted Gd-enhanced MR image of both eyes temporally averaged at approximately 1 hour after intraperitoneal Gd injection from the saline sham control group, showing basic rat eye anatomy (anterior chamber [AC], vitreous body, and lens) and definitions of regions of interest (ROIs) in the anterior chamber and vitreous (*yellow*). Hyperintensity was observed in the anterior chamber but was not apparent in the vitreous because of the entrance and accumulation of the small-molecular-weight Gd contrast agent via the highly permeable blood–aqueous barrier but not the aqueous–vitreous or blood–retinal barrier.

Figure 4 shows the mean fitted time courses of Gd signal enhancement in the anterior chamber and vitreous body of each eye of all groups. Quantitative assessments of Gd signal time courses in terms of peak percentage Gd signal enhancement, initial rate of signal increase within the first 10 minutes after Gd injection, time to peak, and the area under the curve are shown in Figure 5. Due to the limited Gd signal changes in the vitreous body, only the peak percentage Gd signal enhancement and the area under the curve were assessed quantitatively in the vitreous body. The treated right anterior chamber in the microbead group had a 151 ± 36% increase in peak Gd intensity relative to baseline and a 4.1 ± 2.0%/minute initial increase rate, both of which were significantly higher than in the untreated left anterior chamber (paired *t*-tests, $P < 0.05$). Significantly shorter time to peak was also observed in the right anterior chamber (63 ± 14 minutes) relative to the left anterior chamber (75 ± 9 minutes) in the microbead group (paired *t*-test, $P < 0.05$). In contrast, the treated right anterior chamber in the latanoprost group had lower peak intensity (100 ± 37%), lower initial increase rate (1.8 ± 0.9%/minute), and longer time to peak (74 ± 22 minutes) than the untreated left anterior chamber (136 ± 39%, 4.0 ± 1.7%/minute, and 51 ± 16 minutes, respectively; paired *t*-tests, $P < 0.05$). Relative to the latanoprost group, the timolol group showed similar and marginally significant trends (paired *t*-tests between contralateral eyes, $P = 0.055$–0.2). For the brimonidine group, both left and right anterior chambers had the highest peak intensity (~200%), the lowest initial increase rate, and a delayed time to peak relative to all other groups (ANOVA and post hoc Tukey's tests, $P < 0.05$). The area under the curve followed trends similar to those for peak intensity measurement. No significant difference was observed in peak intensity in the untreated left anterior chamber among the microbead, latanoprost, timolol, and saline groups (post hoc Tukey's tests, $P > 0.05$). Initial rate of Gd signal increase in the left anterior chamber in the

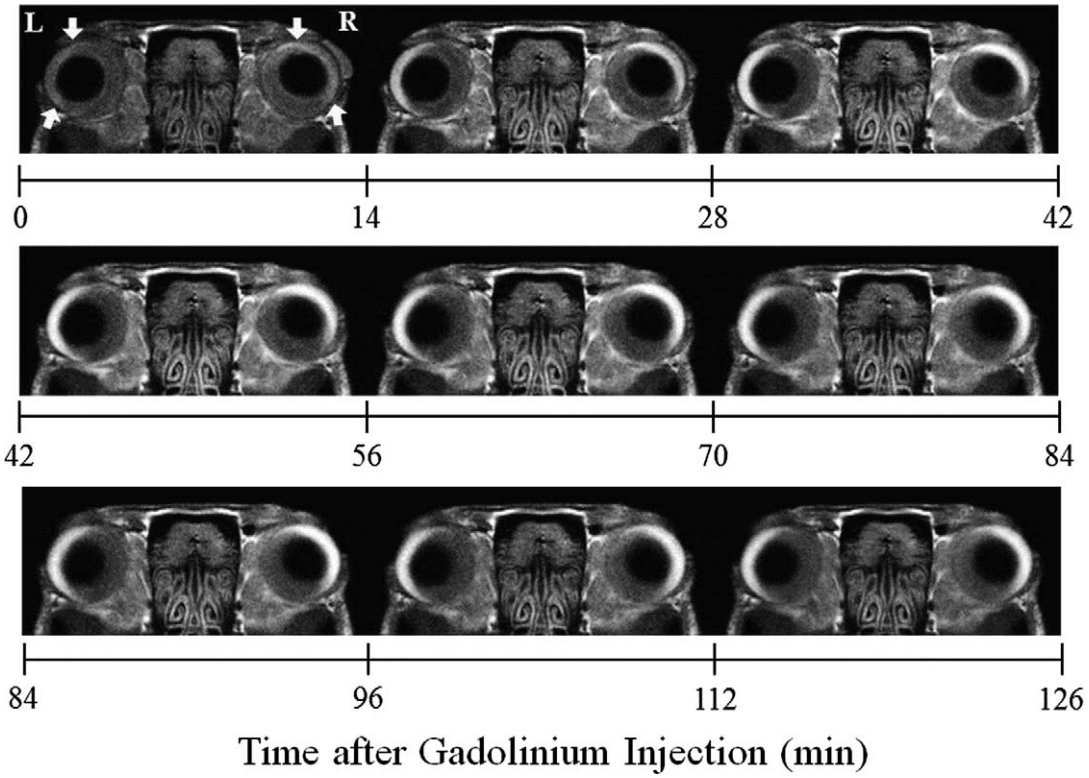

FIGURE 3. Serial T1-weighted Gd-enhanced MR images of both eyes temporally averaged at nine different time intervals from the saline sham control group, showing differential spatiotemporal Gd enhancement profiles in different ocular components. Upon systemic Gd administration, Gd entered the bloodstream and passed the blood–aqueous barrier but not apparently the aqueous–vitreous or blood–retinal barrier. As Gd diffused and followed aqueous humor flow, it accumulated in the anterior chamber (*arrows*), resulting in increasing T1-weighted MRI signal enhancement within the first hour after Gd administration.

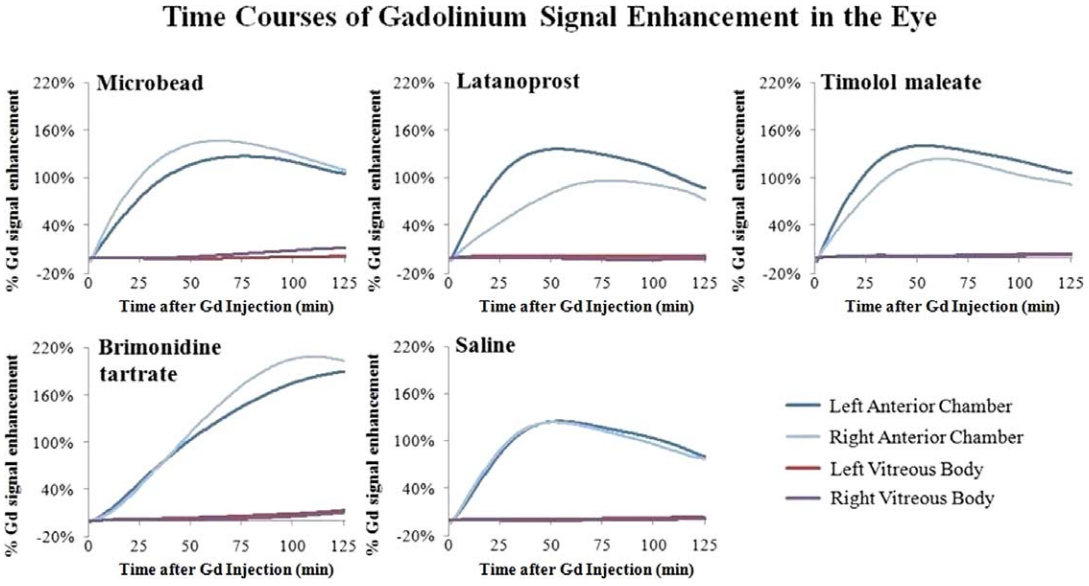

FIGURE 4. Mean fitted time courses of percentage (%) change in T1-weighted Gd signal enhancement in the anterior chamber (AC) and vitreous body of each eye in microbead-, latanoprost-, timolol-, brimonidine-, and saline-treated groups after systemic administration of Gd at 0 minutes. Qualitative evaluation revealed that the time course for the treated right anterior chamber in the microbead group skewed leftward with a higher peak intensity compared to the untreated left anterior chamber. There was also a mild Gd signal enhancement in the right vitreous relative to the left vitreous of the microbead group at approximately 2 hours after Gd injection. The Gd signal time courses for the treated right anterior chamber of the latanoprost and timolol groups skewed rightward with a lower peak intensity compared to the untreated left anterior chamber. For the brimonidine group, both left and right anterior chamber time courses possessed the strongest peak Gd signal enhancement and the longest time to peak compared to other groups. No apparent differences were observed in the saline control group between contralateral eyes or in the left control eyes between microbead, latanoprost, and timolol groups.

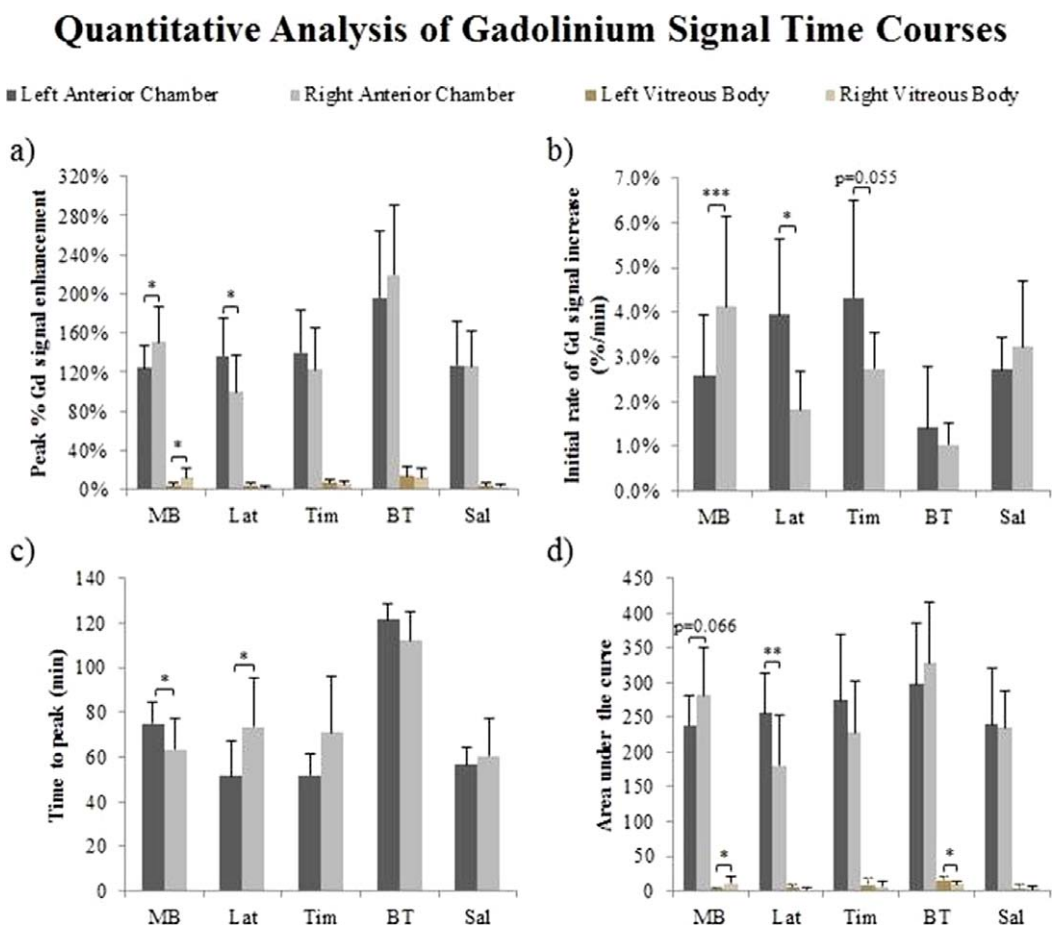

Figure 5. Quantitative comparisons of (**a**) peak percentage (%) change in T1-weighted Gd signal enhancement (in anterior chamber [AC] and vitreous), (**b**) initial rate of Gd signal increase (in AC only), (**c**) time to peak (in AC only), and (**d**) area under the curve (in AC and vitreous) of Gd signal time courses in all microbead (MB), latanoprost (Lat), timolol maleate (Tim), brimonidine tartrate (BT), and saline (Sal) groups (paired *t*-tests between treated and untreated eyes, $^{*}P < 0.05$, $^{**}P < 0.01$, $^{***}P < 0.001$). The treated right anterior chamber in the microbead group had significantly higher peak intensity, higher initial increase rate, shorter time to peak, and marginally larger area under the curve than the untreated left anterior chamber. In contrast, the treated right anterior chamber in the latanoprost group had significantly lower peak intensity, lower initial increase rate, longer time to peak, and smaller area under the curve than the untreated left anterior chamber. Relative to the latanoprost group, the timolol group showed similar and marginally significant trends (paired *t*-tests between contralateral eyes, $P = 0.055$–0.2). For the brimonidine group, both left and right anterior chamber showed significantly higher peak intensity, lower initial increase rate, and delayed time to peak relative to the untreated left anterior chamber in the microbead, latanoprost, timolol, and saline groups (ANOVA and post hoc Tukey's tests, $P < 0.05$). The area under the curve follows trends similar to those for peak intensity measurement. For vitreous body measurements between contralateral eyes, only the microbead group showed significantly stronger Gd enhancement in the right vitreous compared to the left vitreous. It is also noted that the vitreous of both treated and untreated fellow eyes in the brimonidine group had enhanced Gd signals by the end of the experimental period (post hoc Tukey's tests between brimonidine and latanoprost, timolol, and saline groups; left eye $P < 0.05$, right eye $P = 0.08$–0.28). Significant differences in the area under the curve between left and right vitreous were found in both the microbead and brimonidine groups. In the untreated left anterior chamber, no significant difference was observed in the peak intensity among the microbead, latanoprost, timolol, and saline groups (ANOVA, $P > 0.05$). However, time to peak in the left anterior chamber appeared higher in the microbead group than in the latanoprost, timolol, and saline groups (ANOVA and post hoc Tukey's tests, $P < 0.05$), whereas the initial increase rate for the untreated left anterior chamber in the latanoprost and timolol groups appeared higher than in the microbead and saline groups (ANOVA, $P = 0.16$–0.38).

latanoprost and timolol groups appeared higher than in the microbead and saline groups (post hoc Tukey's tests, $P = 0.16$–0.38), whereas the time to peak in the left anterior chamber appeared higher in the microbead group than in the latanoprost, timolol, and saline groups (post hoc Tukey's tests, $P < 0.05$). For vitreous body measurements between contralateral eyes, only the microbead group showed significantly stronger Gd enhancement, by 12 ± 9%, in the right vitreous compared to the left vitreous (paired *t*-test, $P < 0.05$). It is also noted that the vitreous of both treated and untreated fellow eyes in the brimonidine group had higher T1-weighted signal intensities by the end of the experimental period relative to the left control eyes in the latanoprost, timolol, and saline groups (post hoc Tukey's tests; left eye $P < 0.05$, right eye $P = 0.08$–0.28).

Because of the significant Gd enhancement observed in the vitreous body after microbead occlusion and brimonidine treatment, more detailed assessments of the route of Gd entrance in the vitreous body in these two groups were performed, and the results are shown in Figures 6 and 7. While rapid Gd enhancement was observed in the anterior chamber of all eyes, more gradual Gd leakage into the vitreous body was found in the microbead-induced hypertensive right eye as well as both brimonidine-treated and the fellow untreated eyes. Gadolinium predominantly leaked into the anterior vitreous more than the posterior vitreous with a shorter Gd onset time for both microbead-induced hypertensive right eye and

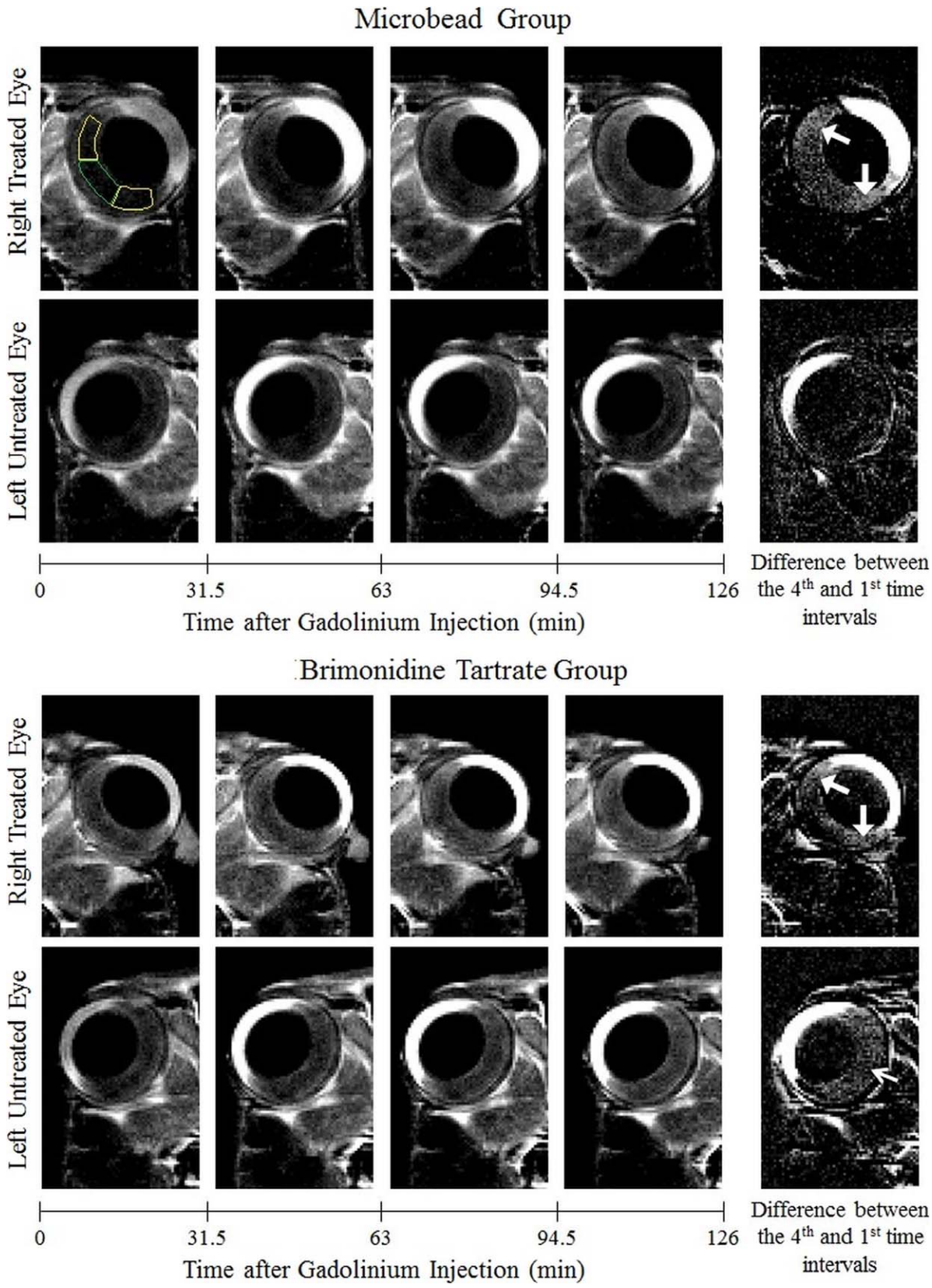

Figure 6. Enlarged T1-weighted Gd-enhanced serial MR images of the eyes temporally averaged at four different time intervals (*left four columns*) and images of signal differences between the fourth and first time intervals (*rightmost column*) in the microbead (*top*)- and brimonidine tartrate (*bottom*)-treated groups. The anterior and posterior portions of the vitreous body are defined and delineated by the *yellow* and *green* regions of interest, respectively. While rapid and significant Gd enhancement was observed in the anterior chamber, gradual Gd leakage into the vitreous body was found in the microbead-induced hypertensive right eye as well as both brimonidine-treated and fellow untreated eyes, but not the untreated left eye in the microbead group or in either eye of the latanoprost-, timolol-, or saline-treated groups (not shown). Gd preferentially leaked into the

Investigative Ophthalmology & Visual Science

anterior vitreous (*closed arrows*) of both the microbead-induced hypertensive right eye and brimonidine-treated right eye, suggestive of the compromise of aqueous–vitreous barrier integrity upon experimental chronic ocular hypertension. More homogenous Gd leakage was observed in the vitreous of the untreated left eye in the brimonidine group (*open arrow*). Together with the higher peak Gd intensity in the anterior chamber of both treated and untreated eyes in the brimonidine group relative to all other groups, these observations may suggest compromise of the blood–ocular and aqueous–vitreous barrier integrity as a potential systemic effect upon unilateral topical application of brimonidine. Note also the apparently larger cross-sectional area of the right anterior chamber versus the left anterior chamber in the microbead group.

brimonidine-treated right eye (paired *t*-tests, $P < 0.05$), suggestive of a compromise of aqueous–vitreous barrier integrity. Despite significantly stronger Gd enhancement in the vitreous body of the untreated left eye in the brimonidine group compared to all other groups, no significant difference in Gd onset time was observed between anterior and posterior vitreous of the left eye. The onset time of Gd enhancement in the posterior vitreous was shorter in the untreated left eye than in the treated right eye in the brimonidine group (paired *t*-test, $P < 0.05$). The cross-sectional area of the anterior chamber in the microbead group appeared larger in the right eye than in the left eye by 33.4% (paired *t*-test, $P < 0.05$).

Discussion

Our results demonstrated that Gd-MRI of the eye can be used to measure spatiotemporally the aqueous humor dynamics and ocular tissue permeability upon altered IOP in an experimental model of chronic glaucoma and during pharmacologic manipulations. The aqueous humor fills the anterior and posterior chambers, constituting a transparent medium for the optical system and acting as a blood surrogate bathing the avascular structure such as the lens and the cornea. It is mainly secreted by the ciliary epithelium lining on the ciliary processes and circulates through the pupil.[29] Upon systemic administration, Gd acts as a passive tracer for the aqueous humor and enters the posterior chamber via the blood–aqueous barrier,[20,22] whereas the aqueous–vitreous and blood–retinal barriers are generally impermeable to Gd in normal adult eyes.[23,25] As Gd diffuses and follows aqueous humor flow, it accumulates in the anterior chamber and causes increasing T1-weighted MRI signal enhancement (Figs. 2, 3, 6).[20,30] At the same time, Gd may be gradually cleared through two known aqueous outflow pathways: the conventional pathway via the circumferential Schlemm's canal[31] and the nonconventional or uveoscleral pathway via the uveal meshwork and the anterior face of ciliary muscle.[32] Depending on the flow dynamics, different states of ocular physiology may give different Gd signal time courses as shown in this study. Initial rate of Gd signal increase, peak Gd signal enhancement, time to peak, and the area under the curve in the Gd signal

a)

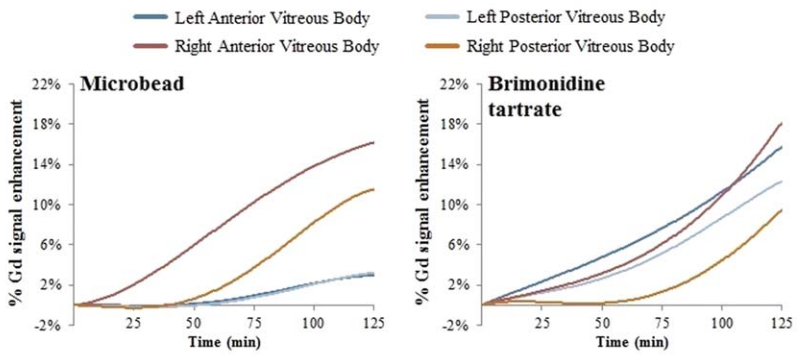

b)

Gadolinium Onset Time (min)

	Left anterior vitreous body	Left posterior vitreous body	Right anterior vitreous body	Right posterior vitreous body
Microbead Group	86.5±50.2#	89.5±52.1	20.5±7.4*	59.2±15.6
Brimonidine Tartrate Group	16.2±9.1	31.5±12.3#	26.5±11.2*	77.4±13.3

Figure 7. (**a**) Mean fitted time courses of percentage (%) change in T1-weighted Gd signal enhancement in the anterior and posterior vitreous body of each eye in the microbead- and brimonidine-treated groups after systemic administration of Gd at 0 minutes. (**b**) Quantitative comparisons of the Gd onset time, defined as when Gd signal enhancement reached 2% of baseline values, showed significantly shorter Gd onset time in the anterior than in the posterior vitreous of the right eyes in both the microbead and brimonidine groups (paired *t*-tests, $*P < 0.05$), which echoes with the potential compromise of aqueous–vitreous barrier integrity leading to Gd flow in the vitreous in an anterior to posterior direction. Despite significantly stronger Gd enhancement in the vitreous body of the untreated left eye in the brimonidine group compared to all other groups, no significant difference in Gd onset time was observed between anterior and posterior vitreous of the left eye. The onset time of Gd enhancement in the posterior vitreous was shorter in the untreated left eye than in the treated right eye in the brimonidine group (paired *t*-test, $\#P < 0.05$). Subtle Gd enhancement (3.8 ± 2.6%) in the untreated left vitreous body was observed in the microbead group but did not reach statistical significance compared to values for the latanoprost, timolol, and saline groups (ANOVA, $P > 0.05$) (paired *t*-tests between anterior and posterior vitreous, $*P < 0.05$; paired *t*-tests between left and right eyes, $\#P < 0.05$).

Investigative Ophthalmology & Visual Science

time courses may be helpful for quantitative evaluation of the causalities of altered aqueous humor dynamics and ocular tissue permeability in different eye components with ocular hypertension and antiglaucoma drug treatments.

The microbead-induced rodent model mimics glaucoma in humans via mild and sustained IOP elevation and may result in neurodegenerative changes such as retinal ganglion cell loss and axonal and myelin damages to the optic nerve.[1,2,33,34] Unlike procedures in other glaucoma models such as laser-induced photocoagulation of the trabecular meshwork or the episcleral and limbal veins, the surgical procedures for microbead occlusion cause minimal damage to the anterior segment with no apparent sign of inflammation.[1,2,34] Intracamerally injected microbeads collect in the iridocorneal angle and block the trabecular meshwork and Schlemm's canal, increasing the resistance of aqueous humor outflow.[34] Such an increase in aqueous outflow resistance could reduce Gd clearance in the anterior chamber, as suggested by the leftward skewing of the Gd signal time course in the treated right anterior chamber relative to the untreated left anterior chamber (Fig. 4). The increased accumulation of Gd upon increased outflow resistance by microbead occlusion, as well as the increased capacity of the anterior chamber for Gd, potentially accounts for the higher peak Gd signal enhancement, the higher initial rate of Gd signal increase, and the shorter time to peak in the anterior chamber of the treated right eye. The area under the signal time curve has been often used in pharmacokinetic modeling of Gd concentration–time integral in dynamic contrast-enhanced MRI. In this study, the increase in area under the curve in the treated right anterior chamber of the microbead group may reflect an increase in the overall amount of contrast agents delivered to and retained in the anterior chamber within the stated experimental time period. Apart from altered aqueous humor dynamics in the anterior chamber, chronic ocular hypertension appeared to compromise the aqueous–vitreous barrier integrity, causing Gd to leak into the vitreous body.[23] The significantly shorter Gd onset time in anterior vitreous versus posterior vitreous of the right, hypertensive eye confirmed that the leakage originated in the aqueous–vitreous interface and flowed in an anterior to posterior direction in the vitreous. Gadolinium leakage to the vitreous body from the aqueous–vitreous interface has been observed in experimental newborn rats, when the tight junctions of the blood–ocular barriers were underdeveloped,[35] and in adult rats that underwent neonatal hypoxia-ischemia.[36] A similar phenomenon was also observed in the current microbead-induced rat model and in the laser-induced chronic ocular hypertension rat model.[24] These findings suggest that disruption of the aqueous–vitreous barrier integrity could be a general observation in experimental chronic ocular hypertension. How such disruption may affect the compositions of aqueous and vitreous humors, their interactions with the ocular environment, and their impacts on glaucoma and other related eye disease may be worthy of further investigations in future studies.

Although both latanoprost and timolol maleate can lead to IOP-lowering effects, their pharmacologic mechanisms are known to be different and may be reflected by Gd-MRI. Latanoprost is a prostaglandin $F_{2\alpha}$-receptor analogue that reduces IOP by increasing uveoscleral drainage of the aqueous humor,[9,37,38] whereas timolol is a nonselective beta-adrenergic receptor antagonist that reduces IOP by decreasing aqueous humor formation.[39,40] As latanoprost facilitates uveoscleral outflow, Gd in the anterior chamber was likely drained away faster upon topical application, while reduction of aqueous humor formation after timolol administration would reduce Gd entrance to the anterior chamber. Overall, these effects gave lower peak intensity, lower initial rate of signal increase, delayed time to peak, and reduced area under the Gd signal time courses in the right anterior chamber compared to the left control, in contrast to microbead-induced ocular hypertension. While the uveoscleral route is characterized by a constant outflow rate in a wide range of IOP,[41] the conventional outflow facility is driven by the difference between IOP and episcleral venous pressure.[42] When IOP is higher than episcleral venous pressure, the pressure difference increases the conventional outflow facility and forces the aqueous humor to drain through the circumferential Schlemm's canal. In contrast, when IOP is below 10 mm Hg, the conventional outflow facility has been shown to decrease to retain the volume of aqueous humor and IOP.[43] With regard to timolol treatment with mean IOP below 10 mm Hg in the current study, reduced aqueous formation with subsequent reduction in conventional drainage might neutralize the expected decreases in Gd entrance and clearance, leading to a smaller net effect on aqueous humor dynamics than the increase in pressure-independent uveoscleral outflow from latanoprost treatment. This may explain why the timolol-treated group showed similar but milder trends toward significance in Gd signal time courses compared to the latanoprost-treated group.

Brimonidine is a selective alpha-2 adrenergic agonist known to reduce aqueous formation and at the same time facilitate uveoscleral outflow.[44] It can be taken orally or topically, and it readily crosses the blood–ocular and blood–brain barriers, interacting with central nervous system (CNS) receptors.[45,46] Unlike oral administration, topical administration bypasses hepatic first-pass metabolism because drugs enter the circulatory system directly through conjunctiva or lacrimal ducts. This bypass path may lead to a relatively larger amount of pharmaceutical entering the circulatory system compared with oral administration[47] and may potentially lead to adverse side effects in the circulatory system and the CNS.[46,48–52] Systemic cardiovascular effects such as hypotension and bradycardia[45,53] and CNS depression[54,55] have been reported as side effects of brimonidine topical administration especially in infants and children. Although the IOP of the treated right eye remained significantly lower than that of the left control eye, similar to observations in previous reports,[56] the underlying reasons for the drastic differences in Gd signal time courses in both eyes of the brimonidine-treated group compared to all other groups are currently unclear; nevertheless, they suggest significant systemic absorption and transfer of antiglaucoma agent to the fellow eye (the consensual ophthalmotonic reaction),[57] cardiovascular effect of brimonidine administration, and involvement of unexplored aqueous humor pathways other than suppression of inflow or facilitation of outflow[58] that may predominate in IOP alteration. Together with the higher peak Gd intensity in the anterior chamber of both treated and untreated eyes in the brimonidine group compared to all other groups, the Gd leakage into the vitreous of both eyes of the brimonidine-treated group also suggests a systemic effect on blood–ocular and aqueous–vitreous barrier integrity in both eyes after unilateral topical application of brimonidine.[56,59,60] In this Gd-MRI study, all treatments were applied to the right eye, and the left eye served as an internal control. In addition, the saline sham control Gd-MRI experiment was performed on six rats selected from the three ocular hypotensive drug groups at 3 weeks after the first Gd-MRI experiment, with no apparent difference observed between the saline-treated eye and the fellow eye. However, subtle differences were observed in the initial rate of Gd signal increase and time to peak in the anterior chamber of the untreated left eyes among the microbead, latanorpost, timolol, and saline groups. This may reflect the potential unilateral treatment effect on aqueous humor dynamics in the untreated eyes.

Gadolinium is a Food and Drug Administration–approved MR contrast agent for human use. Dynamic ocular Gd-MRI technique has also been successfully demonstrated in healthy human subjects[22] and patients with eye diseases,[61,62] and may be directly applicable to glaucoma patients, although cautions are warranted for use in renal patients because of potential complications from high-dose Gd administration on renal functions.[63] In future studies the noninvasiveness and capability for spatiotemporal characterizations of ocular physiology by Gd-MRI together with other brain MRI techniques[64,65] on the visual system may provide an effective, comprehensive, and precise monitoring method for investigations of the consensual ophthalmotonic reaction phenomenon and the structural and physiological eye–brain relationships of glaucoma progression and protection. Moreover, the proposed Gd-MRI system may be combined with different imaging modalities such as optical imaging systems to provide complementary information for assessing aqueous humor dynamics. For example, while Gd-MRI provides a larger field of view and penetration depth for visualizing and evaluating aqueous humor dynamics in the whole globes systematically, optical coherence tomography may provide higher spatial and temporal resolutions for more focused evaluation of small ocular components such as Schlemm's canal[66,67] and intrascleral aqueous humor outflow.[68] Future studies may employ T1 mapping in addition to the current T1-weighted imaging to determine the changes in rate of aqueous flow in the ocular components using the compartmental diffusion model.[26,69] Future studies may also explore the dose-dependent effect, the diurnal/nocturnal effect, and the systemic effect of long-term topical ophthalmic treatment on Gd signal enhancement using simultaneous physiological monitoring such as systemic blood pressure, episcleral venous pressure, and heart rate measurements so as to better understand the causal relationships between ocular physiology, consensual ophthalmotonic reaction, systemic cardiovascular effects, and CNS degeneration/disorder to improve strategies for glaucoma treatment.

In conclusion, the current results demonstrated the use of ocular Gd-MRI as a noninvasive and sensitive model system to visualize and assess spatiotemporally the aqueous humor dynamics and ocular tissue permeability in different eye components upon IOP alterations. Initial rate of Gd signal increase, peak Gd signal enhancement, time to peak, and area under the curve in the Gd signal time courses may quantitatively reflect altered ocular physiology in the anterior chamber, vitreous, and blood–ocular and aqueous–vitreous barriers upon microbead-induced chronic ocular hypertension. Gadolinium MRI may also allow evaluation of the efficacy of antiglaucoma agents through longitudinal monitoring of the aqueous humor flow in vivo. To date, there are only few methods enabling assessment of the effect in vivo on aqueous humor production and uptake spatiotemporally without depth limitation. Our current method may provide such information and put forward Gd-MRI as a tool to investigate novel, unexplored aqueous humor flow pathways globally within the orbit and the head in future studies. Our results also draw attention to the need to better understand the systemic effects of unilateral topical ophthalmic hypotensive drug applications on both treated and untreated eyes during glaucoma treatment.

Acknowledgments

Supported by National Institutes of Health Contracts P30-EY008098 and UL1-TR000005 (Bethesda, Maryland, United States); BrightFocus Foundation Grant G2013077 (Clarksburg, Maryland, United States), Eye and Ear Foundation (Pittsburgh, Pennsylvania, United States); and Research to Prevent Blindness (New York, New York, United States).

Disclosure: **L.C. Ho**, None; **I.P. Conner**, None; **C.-W. Do**, None; **S.-G. Kim**, None; **E.X. Wu**, None; **G. Wollstein**, None; **J.S. Schuman**, None; **K.C. Chan**, None

References

1. Sappington RM, Carlson BJ, Crish SD, Calkins DJ. The microbead occlusion model: a paradigm for induced ocular hypertension in rats and mice. *Invest Ophthalmol Vis Sci*. 2010;51:207–216.
2. Chen H, Wei X, Cho KS, et al. Optic neuropathy due to microbead-induced elevated intraocular pressure in the mouse. *Invest Ophthalmol Vis Sci*. 2011;52:36–44.
3. Chan KC, Fu QL, Hui ES, So KF, Wu EX. Evaluation of the retina and optic nerve in a rat model of chronic glaucoma using in vivo manganese-enhanced magnetic resonance imaging. *NeuroImage*. 2008;40:1166–1174.
4. Chan KC, So KF, Wu EX. Proton magnetic resonance spectroscopy revealed choline reduction in the visual cortex in an experimental model of chronic glaucoma. *Exp Eye Res*. 2009;88:65–70.
5. Chan KC, Li J, Kau P, et al. In vivo retinotopic mapping of superior colliculus using manganese-enhanced magnetic resonance imaging. *NeuroImage*. 2011;54:389–395.
6. Kingman S. Glaucoma is second leading cause of blindness globally. *Bull World Health Organ*. 2004;82:887–888.
7. King A, Migdal C. Clinical management of glaucoma. *J R Soc Med*. 2000;93:175–177.
8. Brubaker RF, McLaren JW. Uses of fluorophotometry in glaucoma research. *Ophthalmology*. 1985;92:884–890.
9. Dinslage S, Hueber A, Diestelhorst M, Krieglstein G. The influence of Latanoprost 0.005% on aqueous humor flow and outflow facility in glaucoma patients: a double-masked placebo-controlled clinical study. *Graefes Arch Clin Exp Ophthalmol*. 2004;242:654–660.
10. Camelo S, Shanley AC, Voon AS, McMenamin PG. An intravital and confocal microscopic study of the distribution of intracameral antigen in the aqueous outflow pathways and limbus of the rat eye. *Exp Eye Res*. 2004;79:455–464.
11. Carreras FJ, Porcel D, Gonzalez-Caballero F. Expanding forces in aqueous outflow pathways of a nonaccommodating mammal: an approach via comparative dynamic morphology. *Comp Biochem Physiol A Physiol*. 1997;117:197–209.
12. Mermoud A, Baerveldt G, Minckler DS, Prata JA Jr, Rao NA. Aqueous humor dynamics in rats. *Graefes Arch Clin Exp Ophthalmol*. 1996;234(suppl 1):S198–S203.
13. Li Y, Cheng H, Shen Q, et al. Blood flow magnetic resonance imaging of retinal degeneration. *Invest Ophthalmol Vis Sci*. 2009;50:1824–1830.
14. Duong TQ. Magnetic resonance imaging of the retina: a brief historical and future perspective. *Saudi J Ophthalmol*. 2011; 25:137–143.
15. Shih YY, Muir ER, Li G, De La Garza BH, Duong TQ. High-resolution 3D MR microangiography of the rat ocular circulation. *Radiology*. 2012;264:234–241.
16. Kim SH, Galbán CJ, Lutz RJ, et al. Assessment of subconjunctival and intrascleral drug delivery to the posterior segment using dynamic contrast-enhanced magnetic resonance imaging. *Invest Ophthalmol Vis Sci*. 2007;48:808–814.
17. Larsson HB, Stubgaard M, Frederiksen JL, Jensen M, Henriksen O, Paulson OB. Quantitation of blood-brain barrier defect by magnetic resonance imaging and gadolinium-DTPA in patients with multiple sclerosis and brain tumors. *Magn Reson Med*. 1990;16:117–131.
18. Ford JC, Wood AK, Van Winkle TJ, Kundel HL. Magnetic resonance imaging observations of blood-brain-barrier perme-

ability in an animal model of brain injury. *Acad Radiol*. 1997;4:115–126.

19. Shen Q, Du F, Huang S, Duong TQ. Spatiotemporal characteristics of postischemic hyperperfusion with respect to changes in T1, T2, diffusion, angiography, and blood-brain barrier permeability. *J Cereb Blood Flow Metab*. 2011;31:2076–2085.
20. Knopp MV, Giesel FL, Marcos H, von Tengg-Kobligk H, Choyke P. Dynamic contrast-enhanced magnetic resonance imaging in oncology. *Top Magn Reson Imaging*. 2001;12:301–308.
21. Henderson E, Sykes J, Drost D, Weinmann HJ, Rutt BK, Lee TY. Simultaneous MRI measurement of blood flow, blood volume, and capillary permeability in mammary tumors using two different contrast agents. *J Magn Reson Imaging*. 2000;12:991–1003.
22. Bert RJ, Caruthers SD, Jara H, et al. Demonstration of an anterior diffusional pathway for solutes in the normal human eye with high spatial resolution contrast-enhanced dynamic MR imaging. *Invest Ophthalmol Vis Sci*. 2006;47:5153–5162.
23. Kolodny NH, Goode ST, Ryan W, Freddo TF. Evaluation of therapeutic effectiveness using MR imaging in a rabbit model of anterior uveitis. *Exp Eye Res*. 2002;74:483–491.
24. Chan KC, Fu QL, Guo H, So KF, Wu EX. GD-DTPA enhanced MRI of ocular transport in a rat model of chronic glaucoma. *Exp Eye Res*. 2008;87:334–341.
25. Alikacem N, Yoshizawa T, Nelson KD, Wilson CA. Quantitative MR imaging study of intravitreal sustained release of VEGF in rabbits. *Invest Ophthalmol Vis Sci*. 2000;41:1561–1569.
26. Berkowitz BA, Roberts R, Luan H, Peysakhov J, Mao X, Thomas KA. Dynamic contrast-enhanced MRI measurements of passive permeability through blood retinal barrier in diabetic rats. *Invest Ophthalmol Vis Sci*. 2004;45:2391–2398.
27. Freddo TF, Patz S, Arshanskiy Y. Pilocarpine's effects on the blood-aqueous barrier of the human eye as assessed by high-resolution, contrast magnetic resonance imaging. *Exp Eye Res*. 2006;82:458–464.
28. Cunha-Vaz J. The blood-ocular barriers. *Surv Ophthalmol*. 1979;23:279–296.
29. Kim H, Robinson MR, Lizak MJ, et al. Controlled drug release from an ocular implant: an evaluation using dynamic three-dimensional magnetic resonance imaging. *Invest Ophthalmol Vis Sci*. 2004;45:2722–2731.
30. Goel M, Picciani RG, Lee RK, Bhattacharya SK. Aqueous humor dynamics: a review. *Open Ophthalmol J*. 2010;4:52–59.
31. Kolodny NH, Freddo TF, Lawrence BA, Suarez C, Bartels SP. Contrast-enhanced magnetic resonance imaging confirmation of an anterior protein pathway in normal rabbit eyes. *Invest Ophthalmol Vis Sci*. 1996;37:1602–1607.
32. Morrison JC, Fraunfelder FW, Milne ST, Moore CG. Limbal microvasculature of the rat eye. *Invest Ophthalmol Vis Sci*. 1995;36:751–756.
33. Cone FE, Gelman SE, Son JL, Pease ME, Quigley HA. Differential susceptibility to experimental glaucoma among 3 mouse strains using bead and viscoelastic injection. *Exp Eye Res*. 2010;91:415–424.
34. Yang Q, Cho KS, Chen H, et al. Microbead-induced ocular hypertensive mouse model for screening and testing of aqueous production suppressants for glaucoma. *Invest Ophthalmol Vis Sci*. 2012;53:3733–3741.
35. Berkowitz BA, Roberto KA, Penn JS. The vitreous protein concentration is increased prior to neovascularization in experimental ROP. *Curr Eye Res*. 1998;17:218–221.
36. Chan KC, Kancherla S, Fan SJ, Wu EX. In vivo assessments of ocular dynamics, axonal transport and microstructural integrity in the visual system after neonatal hypoxic-ischemic injury. *Proc Intl Soc Mag Reson Med*. 2013;21:336.
37. Nilsson SF. The uveoscleral outflow routes. *Eye*. 1997;11(pt 2):149–154.
38. Schachtschabel U, Lindsey JD, Weinreb RN. The mechanism of action of prostaglandins on uveoscleral outflow. *Curr Opin Ophthalmol*. 2000;11:112–115.
39. Zimmerman TJ, Kaufman HE. Timolol. A beta-adrenergic blocking agent for the treatment of glaucoma. *Arch Ophthalmol*. 1977;95:601–604.
40. Radius RL, Diamond GR, Pollack IP, Langham ME. Timolol. A new drug for management of chronic simple glaucoma. *Arch Ophthalmol*. 1978;96:1003–1008.
41. Brubaker RF. Measurement of uveoscleral outflow in humans. *J Glaucoma*. 2001;10:S45–S48.
42. Stamer WD. The cell and molecular biology of glaucoma: mechanisms in the conventional outflow pathway. *Invest Ophthalmol Vis Sci*. 2012;53:2470–2472.
43. Alm A, Nilsson SF. Uveoscleral outflow—a review. *Exp Eye Res*. 2009;88:760–768.
44. Burke J, Schwartz M. Preclinical evaluation of brimonidine. *Surv Ophthalmol*. 1996;41(suppl 1):S9–S18.
45. Bowman RJ, Cope J, Nischal KK. Ocular and systemic side effects of brimonidine 0.2% eye drops (Alphagan) in children. *Eye*. 2004;18:24–26.
46. Carlsen JO, Zabriskie NA, Kwon YH, Barbe ME, Scott WE. Apparent central nervous system depression in infants after the use of topical brimonidine. *Am J Ophthalmol*. 1999;128:255–256.
47. Evans GH, Wilkinson GR, Shand DG. The disposition of propranolol. IV. A dominant role for tissue uptake in the dose-dependent extraction of propranolol by the perfused rat liver. *J Pharmacol Exp Ther*. 1973;186:447–454.
48. Diggory P, Franks W. Glaucoma: systemic side effects of topical medical therapy—a common and under recognized problem. *J R Soc Med*. 1994;87:575–576.
49. Hayes LP, Stewart CJ, Kim I, Mohr JA. Timolol side effects and inadvertent overdosing. *J Am Geriatr Soc*. 1989;37:261–262.
50. Rajan MS, Syam P, Liu C. Systemic side effects of topical latanoprost. *Eye*. 2003;17:442–444.
51. Hegde RR, Bhattacharya SS, Verma A, Ghosh A. Physicochemical and pharmacological investigation of water/oil microemulsion of non-selective beta blocker for treatment of glaucoma. *Curr Eye Res*. 2014;39:155–163.
52. Kiryazov K, Stefova M, Iotova V. Can ophthalmic drops cause central nervous system depression and cardiogenic shock in infants? *Pediatr Emerg Care*. 2013;29:1207–1209.
53. Mungan NK, Wilson TW, Nischal KK, Koren G, Levin AV. Hypotension and bradycardia in infants after the use of topical brimonidine and beta-blockers. *J AAPOS*. 2003;7:69–70.
54. Enyedi LB, Freedman SF. Safety and efficacy of brimonidine in children with glaucoma. *J AAPOS*. 2001;5:281–284.
55. Daubert GP. Is brimonidine ophthalmic a safe therapy for infants? *J Clin Pharm Ther*. 2006;31:289–292.
56. Toris CB, Camras CB, Yablonski ME. Acute versus chronic effects of brimonidine on aqueous humor dynamics in ocular hypertensive patients. *Am J Ophthalmol*. 1999;128:8–14.
57. Gibbens MV. The consensual ophthalmotonic reaction. *Br J Ophthalmol*. 1988;72:746–749.
58. Tam AL, Gupta N, Zhang Z, Yucel YH. Latanoprost stimulates ocular lymphatic drainage: an in vivo nanotracer study. *Trans Vis Sci Technol*. 2013;2:3.
59. Acheampong AA, Shackleton M, John B, Burke J, Wheeler L, Tang-Liu D. Distribution of brimonidine into anterior and posterior tissues of monkey, rabbit, and rat eyes. *Drug Metab Dispos*. 2002;30:421–429.
60. Abdulrazik M, Tamilvanan S, Benita S. Non-systemic delivery of topical brimonidine to the brain: a neuro-ocular tissue distribution study. *J Drug Target*. 2006;14:670–679.

Investigative Ophthalmology & Visual Science

61. Adam G, Brab M, Bohndorf K, Gunther RW. Gadolinium-DTPA-enhanced MRI of intraocular tumors. *Magn Reson Imaging*. 1990;8:683–689.
62. Kupersmith MJ, Alban T, Zeiffer B, Lefton D. Contrast-enhanced MRI in acute optic neuritis: relationship to visual performance. *Brain*. 2002;125:812–822.
63. Stratta P, Canavese C, Aime S. Gadolinium-enhanced magnetic resonance imaging, renal failure and nephrogenic systemic fibrosis/nephrogenic fibrosing dermopathy. *Curr Med Chem*. 2008;15:1229–1235.
64. Chan KC, Fan SJ, Chan RW, Cheng JS, Zhou IY, Wu EX. In vivo visuotopic brain mapping with manganese-enhanced MRI and resting-state functional connectivity MRI. *Neuroimage*. 2014; 90:235–245.
65. Chan KC, Cheng JS, Fan S, Zhou IY, Yang J, Wu EX. In vivo evaluation of retinal and callosal projections in early postnatal development and plasticity using manganese-enhanced MRI and diffusion tensor imaging. *NeuroImage*. 2012;59:2274–2283.
66. Kagemann L, Wollstein G, Ishikawa H, et al. Identification and assessment of Schlemm's canal by spectral-domain optical coherence tomography. *Invest Ophthalmol Vis Sci*. 2010;51: 4054–4059.
67. Li G, Farsiu S, Chiu SJ, et al. Pilocarpine-induced dilation of Schlemm's canal and prevention of lumen collapse at elevated intraocular pressures in living mice visualized by OCT. *Invest Ophthalmol Vis Sci*. 2014;55:3737–3746.
68. Wang B, Kagemann L, Schuman JS, et al. Gold nanorods as a contrast agent for Doppler optical coherence tomography. *PLoS ONE*. 2014;9:e90690.
69. Smith SD. Measurement of the rate of aqueous humor flow. *Yale J Biol Med*. 1991;64:89–102.

Investigative Ophthalmology & Visual Science